Short-range magnetic ordering in the highly frustrated pyrochlore systems FeF_3 and $Mn_2Sb_2O_7$

J. N. Reimers, J. E. Greedan, C. V. Stager, and M. Bjorgvinnsen
Institute for Materials Research and The McMaster Nuclear Reactor, McMaster University, Hamilton, Ontario, Canada L8S 4M1

M. A. Subramanian
E. I. du Pont de Nemours and Co., Experimental Station, Wilmington, Delaware 19898
(Received 25 October 1990)

FeF_3 and $Mn_2Sb_2O_7$ exhibit long-range magnetic order at 15.5 and 13 K, respectively. Bulk magnetic susceptibility data for these compounds show a strong dependence on sample history and deviations from a Curie-Weiss-law behavior far above the ordering temperatures. These effects are attributed to short-range order over a wide temperature range. Long-range order is inhibited in these compounds by the highly frustrated lattice of corner-sharing tetrahedra formed by the metal (Fe^{3+} and Mn^{2+}) sublattices. Neutron-diffraction data given clear evidence for short-range correlations above T_c. Fourier analysis of the data yields an approximation to the radial distribution function, which is interpreted in terms of spin-spin correlations out to the fourth-neighbor coordination shell. For both compounds we observe strong antiferromagnetic first-neighbor, and ferromagnetic second- and third-neighbor, spin-spin correlations.

I. INTRODUCTION

Pyrochlores have the chemical composition $A_2B_2O_7$ and crystallize in the cubic, face-centered space group $Fd\bar{3}m$, where the A and B atoms are metals located on the sites 16c and 16d of the space group with oxygens occupying the 48f and 8a sites. Each of the metal atoms in this system forms an infinite three-dimensional lattice of corner-sharing tetrahedra. If either of the A or B atoms is magnetic, then there is a very high degree of frustration when the nearest-neighbor interactions are antiferromagnetic. A schematic diagram of the tetrahedra formed by the 16c lattice along with a unit cell is shown in Fig. 1, the 16d sublattice is identical to this except for a spatial displacement of $(\frac{1}{2},\frac{1}{2},\frac{1}{2})$.

The pyrochlore form of FeF_3[1] has lattice constant $a=10.232$ Å with Fe atoms on the 16c site and fluorine at 48f, the 16d and 8a sites are unoccupied. Very little is known about magnetic ordering in pyrochlore antiferromagnets; in fact, FeF_3 is the only such compound for which a low-temperature antiferromagnetic structure has been observed.[1] Here the low-temperature phase consists of four sublattices oriented along the four [111] directions, thus, any two sublattices are oriented at 109° from each other. Signs of short-range order are evident at temperatures on the order of 10 T_c where the susceptibility shows strong deviations from Curie-Weiss behavior.[1]

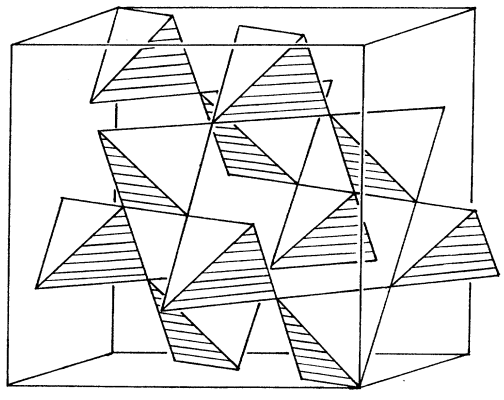

FIG. 1. The three-dimensional network of corner-sharing tetrahedra formed by one of the metal sublattices in pyrochlores. An outline of the cubic unit cell is also shown.

$Mn_2Sb_2O_7$ is actually a distorted form of pyrochlore with the distortion primarily along one of the three-fold axes. To a first approximation the space group is $R\bar{3}m$ (Ref. 2) but further investigations have revealed even lower symmetry of $P3_121$ (Ref. 3) or $P2$ (Ref. 4), which are all successive subgroups. Therefore, the detailed structure of this compound is not known but it is a reasonable assumption that the magnetic sublattice of Mn^{2+} atoms forms a slightly distorted version of the corner-sharing tetrahedral lattice in normal pyrochlores. Scott[3] has proposed a hexagonal structure, $a=7.191$ Å and $c=17.398$ Å, in the space group $P3_121$, based on x-ray-diffraction data.

The magnetic species in FeF_3 and $Mn_2Sb_2O_7$ is a d^5 ion with a totally symmetric ^6A ground state. In FeF_3 the Fe^{3+} ion is in a roughly octahedral environment with $\bar{3}m$ site symmetry and six equivalent Fe-F distances. Because the exact structure is not known for $Mn_2Sb_2O_7$, it will be assumed that the Mn^{2+} environment is a slightly distorted version of the environment in FeF_3. Because the ions have symmetric ground states with no net orbital angular momentum, any anisotropy will be weak and thus unimportant in the high-temperature regime. However, due to the highly frustrated nature of these systems, any small amount of anisotropy will be important in determining the long-range-ordered state.

A more complete review of the magnetic properties of oxide pyrochlores can be found in Ref. 5. For a detailed discussion of magnetic ordering in pyrochlores as predicted by mean-field theory, see Ref. 6.

In order to understand the nature of the short-range magnetic ordering and also to obtain a rough idea of the microscopic interactions present in these systems, we have performed neutron-diffraction experiments on polycrystalline samples of FeF_3 and $Mn_2Sb_2O_7$. Magnetic susceptibility measurements complement the neutron data and also show evidence for short-range order and frustration.

II. EXPERIMENTAL DETAILS

The preparation of FeF_3 and $Mn_2Sb_2O_7$ is described elsewhere.[1,2] Great care was taken in removing the ammonia from the FeF_3 in order to minimize the incoherent scattering from hydrogen. Powder neutron-diffraction data were obtained at the McMaster Nuclear Reactor with 1.3913-Å neutrons. Data sets at 273, 160, 80, 60, 40, and 20 K were collected for FeF_3 and at 9, 11, 13, 15, 20, 26, 35, 70, and 295 K for $Mn_2Sb_2O_7$. The detector was a three-tube position-sensitive detector which has been described previously.[7] The sample was held in an aluminum can along with helium exchange gas and sealed with an indium gasket.

The high-temperature magnetic susceptibility data for $Mn_2Sb_2O_7$ were collected on a Princeton Applied Research (PAR) vibrating sample magnetometer calibrated with high-purity nickel. All other magnetic susceptibility data were collected on a Quantum Design SQUID magnetometer using a pressed polycrystalline pellet. The SQUID was calibrated with high-purity palladium.

III. RESULTS

A. Magnetic susceptibility FeF_3

As mentioned above, the high-temperature susceptibility has been described elsewhere[1] and will not be discussed further here except to say that no Curie-Weiss-law behavior is observed up to 300 K. Below 120 K the high-field susceptibility (1 T) shows a broad maximum at 85 K (Fig. 2) which is most likely a result of short-range ordering of the Fe^{3+} moments. The minimum at 16 K coincides with the temperature where long-range order sets in.

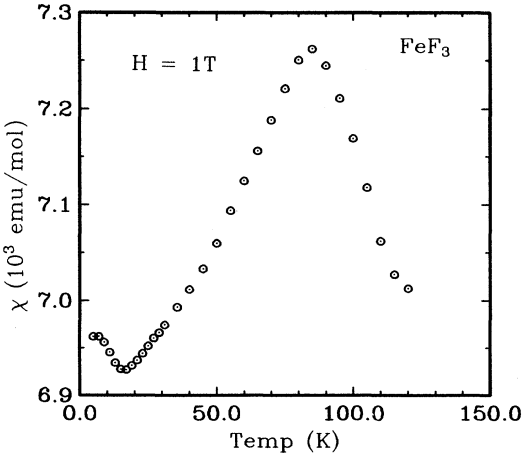

FIG. 2. Low-temperature susceptibility data for FeF_3 measured at an applied field of 1 T on a residual field-cooled sample. The broad maximum at 85 K is ascribed to the onset of strong short-range correlations below 120 K.

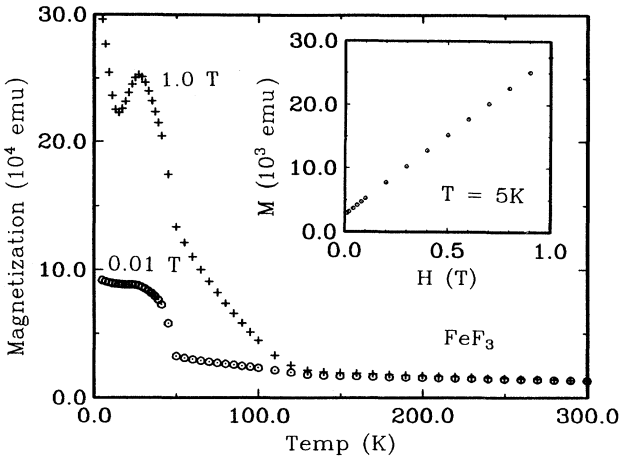

FIG. 3. Magnetization data for FeF_3 showing sample history dependence. The sample was cooled in fields of 1 T (+) and 0.01 T (○) starting at 300 K, then measured while warming in an applied field of 0.01 T. The inset shows the linear behavior of the magnetization with applied field at $T=5$ K.

Further evidence for strong short-range correlations is furnished by sample history dependence at lower temperatures. To see the history dependence, the sample is cooled from the starting temperature down to 5 K in a high field (1 T). The field is then reduced to 0.01 T and the sample is measured while warming, cooled again, and remeasured, with the field fixed at 0.01 T. This procedure ensures that the high-field-cooled (HFC) and low-field-cooled (LFC) runs are both measured with the same applied field. Figure 3 shows the results for a starting temperature of 300 K. The history dependence is seen to persist up to 130 K which is an order of magnitude higher than 15.5 K where long-range order sets in. Just

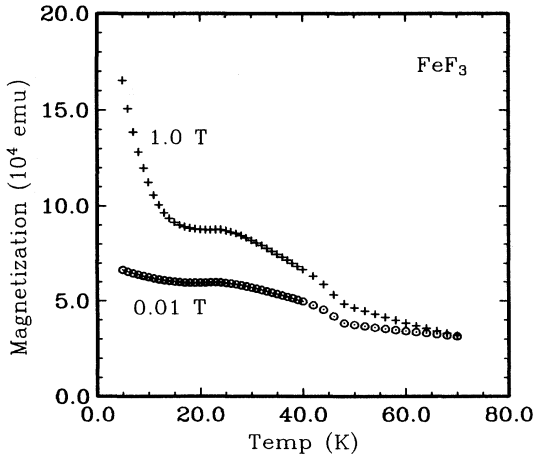

FIG. 4. As in Fig. 2 with a starting temperature of 70 K, which is inside the short-range-order regime.

below 50 K another sharp feature can be seen in both the HFC and LFC runs. The inset in Fig. 3 shows the linear behavior of the magnetization with field at 5 K, indicating that the relaxation time in the sample is smaller than the time scale of the experiment. Figure 4 is similar to Fig. 3, with a starting temperature of 70 K, i.e., here the sample was cooled in residual field (≈ 2 mT) to 70 K before ramping the field up to 1 T. Again, the sharp feature below 50 K is present, however, the strong maximum at ≈ 30 K in the HFC run has been reduced to a plateau. This dramatic history dependence of the magnetization is believed to be due to the onset of strong short-range correlations below about 130 K and the high degree of frustration.

B. Magnetic susceptibility $Mn_2Sb_2O_7$

Figure 5 shows a Curie-Weiss-law plot of the susceptibility data (corrected for diamagnetism) at an applied field of 1 T for $Mn_2Sb_2O_7$, in the temperature range 50–300 K. The least-squares fit yielded an effective moment $\mu = 5.92(1)\mu_B$ as expected for $S = \frac{5}{2}$, and $\theta = -48.9(6)$ K, indicating predominantly antiferromagnetic interactions. Below 50 K the data show deviations from Curie-Weis behavior indicating the onset of short-range order.

Figure 6 shows the sample history dependence for $Mn_2Sb_2O_7$ magnetization data, obtained by employing the same procedure as above with a starting temperature of 70 K. Again the history dependence persists up to 55 K far above the long-range-ordering temperature of 13 K. Thus, we have evidence for the onset of short-range correlations below about 55 K. More detailed information on these correlations can be obtained from the neutron-diffraction experiments.

C. Neutron diffraction FeF_3

In order to isolate the correlated magnetic scattering in low-temperature data sets, the high-temperature (273 K) data set was subtracted thus removing nuclear and paramagnetic scattering. The results are shown in Fig. 7. In order to account for small changes in cell constants, the high-temperature data set was renormalized in **q** space in such a way that the strongest nuclear Bragg reflections would superimpose. The roughening in the data at about 13° in 2θ is due to the presence of a very strong nuclear [111] Bragg reflection. At 20 K one can see that a small amount of Bragg scattering (approximately 5% of the original peak) is left over after the subtraction which can be attributed to changes in the nuclear Debye-Waller factor.

The dominant feature in these data sets is the broad

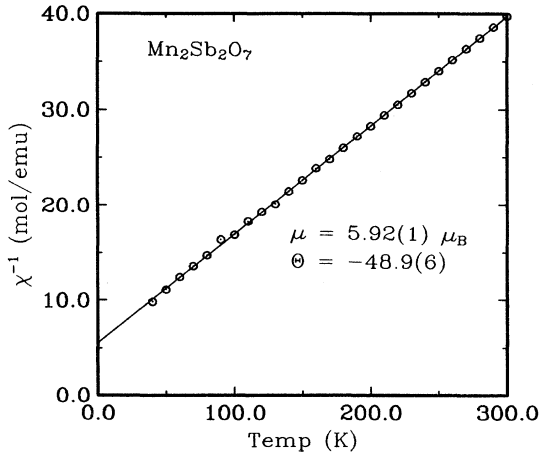

FIG. 5. Curie-Weiss law fit to the inverse susceptibility data for $Mn_2Sb_2O_7$ giving $\mu = 5.92(1)\mu_B$ and $\theta = -48.9(6)$ K.

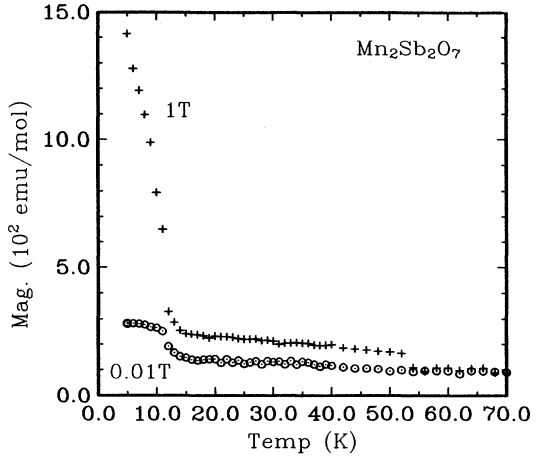

FIG. 6. Magnetization for $Mn_2Sb_2O_7$, following the procedure employed for FeF_3, showing sample history dependence below about 55 K.

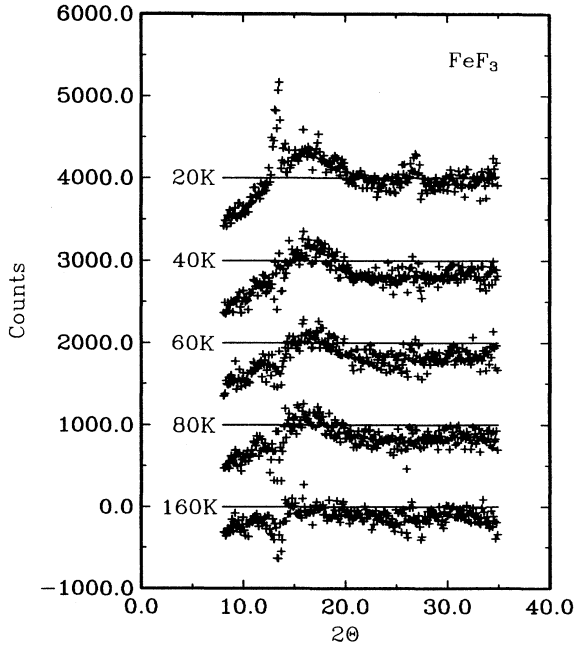

FIG. 7. Neutron-scattering data for FeF_3 showing diffuse scattering due to short-range correlations of Fe^{3+} moments. Nuclear and paramagnetic scattering has been removed by subtracting the high-temperature data set (273 K).

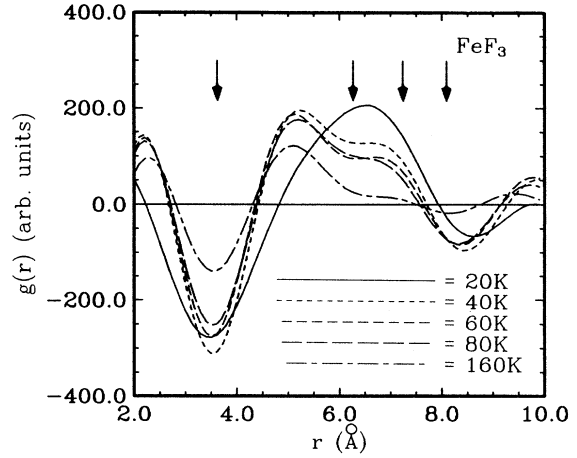

FIG. 8. Real-space radial correlation functions for FeF_3 (in arbitrary units) obtained by Fourier transforming the low-temperature difference data sets. Arrows indicate the four nearest-neighbor bond distances for the Fe^{3+} sublattice.

feature at $\approx 15°$ in 2θ and depletion of scattering near 10° 2θ, resulting from short-range ordering of the Fe^{3+} moments. Significant short-range ordering sets in only below 160 K, which is consistent with susceptibility data.

Better insight into the short-range correlations can be obtained by Fourier transforming the data, which gives the radial correlation function[8]

$$g(r)=\int_{Q_l}^{Q_h} I_{\text{diff}}(Q) f(Q)^{-2} Q \sin(Qr) dQ \ ,$$

where $Q=4\pi\sin(\theta)/\lambda$ is the scattering vector, $I_{\text{diff}}(Q)$ is the magnetic scattering intensity at Q with the paramagnetic scattering subtracted, and $f(Q)$ is the magnetic form factor. In the limit of isotropic interactions

$$g(r)=\frac{1}{S(S+1)}\sum_{r'}\langle \mathbf{S}_0\cdot\mathbf{S}_{r'}\rangle \delta(|\mathbf{r}|-|\mathbf{r}'|) \ ,$$

which is a sum of spin-spin correlations at distance r. Figure 8 shows the Fourier transforms of the five low-temperature data sets. The arrows indicate the first-to fourth-neighbor Fe—Fe bond distances. The main contribution to the error in this sort of analysis is most likely from the limited Q range of the data. Other sources of error such as data noise and anisotropy are less significant.

From Fig. 8 we can see that there are strong antiferromagnetic correlations between first neighbors at all temperatures. Below 80 K ferromagnetic correlations between second and third neighbors develop. Also, the 20-K data set shows qualitative differences from all the other data sets. The resolution provided by this analysis is not good enough to separate the contributions from the second- and third-neighbor correlations.

D. Neutron diffraction $Mn_2Sb_2O_7$

The 300-K difference data for $Mn_2Sb_2O_7$ (Fig. 9) is very similar to that of FeF_3 for the higher temperatures, again having the broad feature near $2\theta\approx 15°$. Below 13 K,

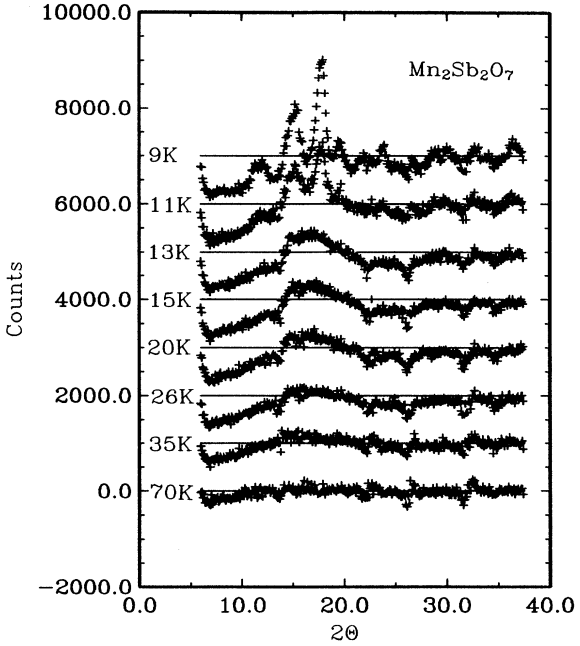

FIG. 9. Neutron-scattering data for $Mn_2Sb_2O_7$ showing diffuse scattering due to short-range correlations of Mn^{3+} moments. Nuclear and paramagnetic scattering has been removed by subtracting the high-temperature data set (295 K).

resolution-limited magnetic Bragg peaks begin to develop. Again, the Fourier analysis (Fig. 10) indicates strong antiferromagnetic first-neighbor, and ferromagnetic second- and third-neighbor, spin-spin correlations. Here the coordination shells are defined within a range of bond distances calculated from Scott's refinement of the crystal structure in the space group $P3_121$.[3]

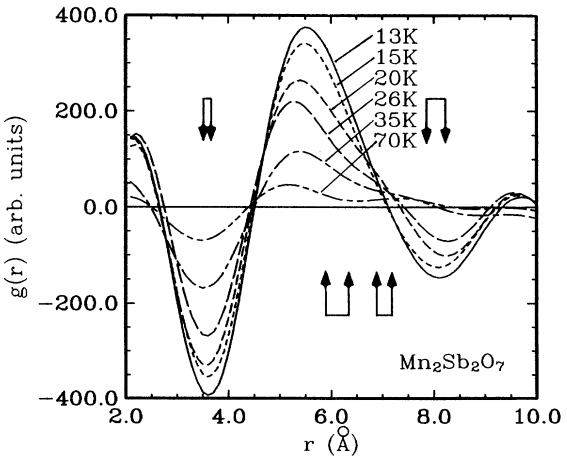

FIG. 10. Real-space radial correlation functions for $Mn_2Sb_2O_7$ (in arbitrary units) obtained by Fourier transforming the low-temperature difference data sets. Arrows indicate upper and lower limits on the four nearest-neighbor coordination shells in the Mn^{2+} sublattice.

TABLE I. Observed and calculated magnetic peak positions for $Mn_2Sb_2O_7$, based on Scott's hexagonal cell.

	Pos. (2θ)	d (Å)	Rel. int.	(hkl)	Calc. pos. (2θ)
1	11.44(2)	6.98(1)	17(1)	$(\frac{1}{2},0,2)$	11.20
2	15.13(2)	5.28(1)	58(2)	$(\frac{1}{2},0,3)$	15.21
3	17.73(1)	4.514(5)	100(2)	$(\frac{1}{2},\frac{1}{2},3)$	17.73
4	19.49(4)	4.11(1)	17(1)	$(\frac{1}{2},0,4)$	19.51
5	22.10(6)	3.63(2)	16(2)	$(\frac{1}{2},1,3)$	21.94
6	23.76(4)	3.37(1)	21(1)	$(\frac{1}{2},\frac{3}{2},1)$	23.70
				$(\frac{3}{2},0,3)$	23.78
7	28.82(7)	2.80(1)	10(1)	$(\frac{1}{2},1,5)$	28.79
8	30.13(6)	2.68(1)	11(1)	$(\frac{1}{2},2,1)$	30.03
				$(\frac{3}{2},0,5)$	30.24

The Bragg peak intensities and positions are listed in Table I. All reflections could be indexed on a unit cell $(2a,2a,c)$ or equivalently with a $(\frac{1}{2},\frac{1}{2},0)$ propagation vector, as related to Scott's hexagonal unit cell. The calculated peak positions within this indexing scheme are also listed in Table I. The lack of detailed crystallographic information on this compound makes the solution of the magnetic structure rather difficult, thus no attempts have been made.

IV. CONCLUSIONS

The neutron-diffraction data show directly that both compounds have nearest-neighbor antiferromagnetic interactions. In the absence of further-neighbor interactions, the pyrochlore system is not expected to order at any temperature[9,10] on the basis of qualitative arguments. Villain calls these systems "cooperative paramagnets".[10] As a result of this, pyrochlore can be expected to develop strong nearest-neighbor antiferromagnetic correlations at temperatures below $|J_1|$, the nearest-neighbor interaction, without long-range order. In some cases further-neighbor interactions will stabilize long-range order at temperatures much lower than $|J_1|$.[6] This is clearly the situation in FeF_3 and $Mn_2Sb_2O_7$.

The strong dependence of the susceptibility data on sample cooling history is more reminiscent of spin-glass behavior than that of chemically ordered magnetic systems. However, a number of pyrochlore compounds have recently been shown to exhibit spin-glass-like behavior in the absence of chemical disorder. $Y_2Mn_2O_7$ (Ref. 11) shows diffuse neutron scattering over a wide temperature range as well as sample history dependence in the susceptibility. Heat-capacity data show no anomalies associated with a phase transition, and the entropy removal is almost 100% down to 2 K.[12] The related compound $Y_2Mo_2O_7$ shows spin-glass-like behavior[13] in the form of a cusp and sample history dependence in the magnetic susceptibility, even though the compound is chemically ordered.[14] The high degree of frustration on the Mn^{4+} and Mo^{4+} sublattices is believed to be responsible for the unusual effects observed in these compounds. Similar behavior has also been observed in susceptibility data for $Tb_2Mo_2O_7$.[15,16] Here spin-glass-like behavior is also evident in neutron-diffraction data where strong diffuse magnetic scattering develops below the apparent freezing temperature of 25 K.

Detailed crystallographic work on $Mn_2Sb_2O_7$ and high-resolution neutron-diffraction data will be required in order solve the low-temperature magnetic structure. The other spin-glass-like systems ($Y_2Mo_2O_7$, $Y_2Mn_2O_7$, and $Tb_2Mo_2O_7$) mentioned above are expected to order at low enough temperatures. Neutron experiments on these compounds below 1 K are also of great interest. Low-temperature observations on field-cooled samples of all the pyrochlores mentioned should also be investigated with neutron diffraction.

ACKNOWLEDGMENTS

We thank Mr G. Hewitson for carrying out the susceptibility measurements. J.N.R. and J.E.G. acknowledge financial assistance from the National Science and Engineering Research Council of Canada.

[1]G. Ferey, R. De Pape, M. Leblanc, and J. Pannetier, Rev. Chim. Miner. **23**, 474 (1986).

[2]M. A. Subramanian, A. Clearfield, A. M. Umarji, G. K. Shenoy, and G. V. Subra Rao, J. Solid State Chem. **52**, 124 (1984).

[3]H. G. Scott, J. Solid State Chem. **66**, 171 (1987).

[4]J. E. Greedan and J. N. Reimers (unpublished). Weak reflections in time-of-flight neutron-diffraction data obtained from the General purpose powder diffractometer at Argonne National Laboratory were only consistent with a large (roughly orthorhombic) unit cell with dimensions $a=7.2$, $b=12.47$, $c=17.42$ Å in the space group $P2$. This is a super cell with double the volume of the one reported by Scott in the space group $P3_121$.

[5]J. E. Greedan, in *Magnetic Properties of Non-Metals,* Vol. III/27 of *Landolt-Bornstein New Series,* edited by H. P. J. Wijn (Springer, Berlin, in press).
[6]J. N. Reimers, A. J. Berlinsky, and A.-C. Shi Phys. Rev. B **43**, 865 (1981).
[7]J. N. Reimers, J. E. Greedan, and M. A. Subramanian, J. Solid State Chem. **79**, 263 (1989); J. N. Reimers and J. E. Greedan, *ibid.* **72**, 390 (1988).
[8]E. F. Bertaut and P. Burlet, Solid State Commun. **5**, 279 (1967).
[9]P. W. Anderson, Phys. Rev. **102**, 1008 (1956).
[10]J. Villain, Z. Phys. B **33**, 31 (1978).
[11]M. A. Subramanian, C. C. Torardi, D. C. Johnson, J. Pannetier, and A. W. Sleight, J. Solid State Chem. **72**, 24 (1988).
[12]J. N. Reimers, J. E. Greedan, R. K. Kremer, E. Gmelin, and M. A. Subramanian, Phys. Rev. B (to be published).
[13]J. E. Greedan, M. Sato, X. Yan, and F. S. Razavi, Solid State Commun. **59**, 895 (1986).
[14]J. N. Reimers and J. E. Greedan, J. Solid State Chem. **72**, 390 (1988).
[15]J. N. Reimers, J. E. Greedan, S. L. Penny, and C. V. Stager, J. Appl. Phys. **67**, 5967 (1990).
[16]J. E. Greedan, J. N. Reimers, C. V. Stager, and S. L. Penny, preceding paper, Phys. Rev. B **43**, 5682 (1991).